A 2-Hydroxy-1-Naphthaldehyde Schiff Base for Turn-on Fluorescence Detection of Zn2+ based on PET Mechanism

Xinyue Mu
Guilin University of Technology
Liping Shi
Guilin University of Technology
Liqiang Yan (liqiangyan@glut.edu.cn)
Guilin University of Technology https://orcid.org/0000-0002-4633-4028
Ningli Tang
Guilin University of Technology

Research Article

Keywords: Fluorescence analysis, Schiff base, Zn2+, Water sample, Cell imaging

Posted Date: March 15th, 2021

DOI: https://doi.org/10.21203/rs.3.rs-285879/v1

Version of Record: A version of this preprint was published at Journal of Fluorescence on April 16th, 2021. See the published version at https://doi.org/10.1007/s10895-021-02732-1.

Abstract

Zinc ion is closely related to human health. Its content in human body is small, while the effect is large. However, it is not the more the better, must be in a scientific balance. Therefore, it is significant to the rapid detection of Zn^{2+} in the environment and organism. Herein, a fluorescent probe based on 2-hydroxy-1-naphthalene formaldehyde and furan-2-carbohydrazide was conveniently synthesized via Schiff base reaction. And this probe has been successfully applied to the accurate and quantitative detection of Zn^{2+} in real samples, showing turn on fluorescence, good selectivity, very low detection limit, real time response and reusability. In addition, this probe has the potential application to trace Zn^{2+} in living cells with low cytotoxicity.

1. Introduction

Zinc ions (Zn^{2+}), as one of the essential trace elements related to human's growth and health, exists in many of the enzymes [1–5]. Many physiological processes are inseparable from the participation of Zn^{2+}, such as gene transcription, bio-signal transduction, intelligence development, cell immune [6–8]. Zinc deficiency will lead to neuronal death, hypertension, chronic kidney disease and worsens kidney complications, oxidative stress, growth retardation and hypogonadism [9–14]. Zinc is a necessary trace element in the body, the content is small, and the effect is large. However, it is not the more the better, must be in a scientific balance. A large amount of Zn^{2+} can inhibit the activity and bactericidal force of phagocytes, thereby reducing the immune function of the human body [15]. In addition, the ratio of Zn^{2+}/Cu^{2+} in the human body has a normal range. Due to the increase of Zn^{2+}/Cu^{2+} ratio caused by a large amount of Zn^{2+} supplementation, cholesterol metabolism in the body is disturbed, resulting in hypercholesterolemia, which leads to hypertension and coronary heart disease [16]. Large doses of Zn^{2+} preparation can cause zinc poisoning, resulting in toxic effect on digestive and nerve systems, and even causing cancer [17]. Therefore, the rapid detection of Zn^{2+} in the environment and organisms has important practical significance.

At present, a variety of Zn^{2+} detection and analysis methods have been developed, including electron mobility sensor, gravimetric method, colorimetric method, polarographic method and flame atomic absorption spectrophotometry [18–22]. However, these methods have some unavoidable disadvantages that hinder their application for rapid detection, such as the troublesome procedures, serious interference from other elements, the participation of inert gas, professional operation technology and being difficult to realize real time detection.

Optical analysis technology based on small organic molecules has outstanding advantages such as high sensitivity, good selectivity, simple detection equipment, visualization, etc., and has developed into a powerful tool for molecular biology, cell biology, analytical chemistry, environmental detection and clinical diagnosis [23–25]. During recent years several probes based on small organic fluorophores have been developed, and successfully used in the detection of Zn^{2+} in aqueous environments and living cells [26–

35]. However, the fluorescent probes with fast response time, low cytotoxicity and wide application range still need to be further developed to realize the determination of this metal ion (Table S1). Herein, a fluorescent probe with specific selectivity and high sensitivity for the simple and rapid detection of Zn^{2+} in oral zinc supplements, drinking water and living cells was established (Scheme 1).

2. Experimental

2.1. Materials and Equipment

2-hydroxy-1-naphthalene formaldehyde (98%), furan-2-carbohydrazide (98%), HEPES and ethylenediamine tetraacetic acid disodium salt (EDTA-2Na) were purchased from Sun Chemical Technology (Shanghai) Co., Ltd. and used directly. All solvents (AR) were provided by market suppliers and did not special process. The water through the experiment was deionized water. Common metal ions and anions were prepared using their nitrates and sodium salts, respectively.

The structures of the compounds were identified using nuclear magnetic resonance spectra (NMR) and high resolution mass spectra (HRMS). The detection performances of the probe were evaluated by UV-visual absorption and fluorescence spectra.

2.2. Spectral measurements

UV-visual absorption and fluorescence spectra were acquired in CH_3CN/HEPES (1/1, v/v, pH 7.2) at room temperature. The slit width and the excitation wavelength (λ_{ex}) of fluorescence spectra were set to 10 nm/10 nm and 428 nm, respectively.

2.3. Synthesis of probe NFC

2-hydroxy-1-naphthalene formaldehyde (0.2 mmol, 35 mg) and furan-2-carbohydrazide (0.2 mmol 25.2 mg) were dissolved in anhydrous C_2H_5OH (10 mL) and stirred at reflux for 3 h. After the solution was cooled to room temperature, the precipitate was collected by suction filtration, and washed 2–3 times with ice C_2H_5OH to obtain pale yellow solid (25 mg, Yield, 44.6%). ^{1}H NMR (DMSO-d_6) δ: 12.65 (s, 1H), 12.24 (s, 1H), 9.52 (s, 1H), 8.24–8.22 (d, J = 10 Hz, 1H), 8.03 (s, 1H), 7.96–7.94 (d, J = 10 Hz, 1H), 7.92–7.90 (d, J = 10 Hz, 1H), 7.64–7.61 (t, J = 7.5 Hz, 1H), 7.44–7.41 (t, J = 7.5 Hz, 1H), 7.36–7.35 (d, J = 5Hz, 1H), 7.25–7.23 (d, J = 10 Hz, 1H), 6.77–6.76 (d, J = 5Hz, 1H). ^{13}C NMR (DMSO-d_6) δ: 158.41, 154.15, 147.53, 146.65, 133.28, 132.08, 129.46, 128.29, 124.06, 121.17, 119.35, 115.96, 112.83, 109.03. HR-MS (m/z): found 281.0928 ($[M + H]^+$), 304.0782 ($[M + Na]^+$), calcd for $C_{16}H_{12}N_2O_3$ 280.0848.

2.4. Fluorescence imaging

HepG2 cells, purchased from market supplier (China Center for Type Culture Collection (CCTCC)), were cultured in DMEM with 10% fetal bovine serum (FBS) at 37°C. HepG2 cells were first treated with 10 μM probe NFC for 30 min, and further cultured with 20 μM Zn^{2+} for 20 min. Then the treated cells were

washed with PBS three times and fluorescence images were acquired using laser scanning confocal microscope.

Cytotoxicity assay was evaluated by MTT assay. A549 cells supplied by CCTCC were placed in a 96-well plate and adhered for 24 h. Subsequently, the cells were added with a series concentrations of probe NFC (0, 10, 20, 30, 40, 50 μM) and cultured for another 24h. After staining with the MTT formazan (5 mg/mL) for 4 h, the absorbance value was measured at 470 nm.

2.5. Treatment process of real water samples

The detection ability in real water samples was evaluated in pond water and drinking water, respectively. HEPES were respectively dissolved in these pond water and drinking water, and adjusted the pH value to 7.2. These the HEPES buffer solutions prepared from tap water and pond water were mixed with CH_3CN (CH_3CN/HEPES buffer, 1/1, v/v), respectively. Then different concentrations of Zn^{2+} and the stock solution of probe NFC were added into the water samples. After equilibrium for 2 min, their fluorescence spectra were tested. The commercial zinc supplement (calcium and zinc gluconate oral solution) was made in Hubei noon time pharmaceutical co., LTD of China. The calcium and zinc gluconate oral solution was diluted 2000 times with CH_3CN/HEPES buffer and added directly to the probe solution.

3. Results And Discussion

3.1. Optical behavior of probe NFC with Zn^{2+}

UV-Vis absorption spectra of probe NFC (10 μM) with increasing content of Zn^{2+} (0–17 μM) were collected in CH_3CN/HEPES (1/1, v/v, pH 7.2). The solution of probe NFC only showed three absorption bands, located at 262 nm, 325 nm and 362 nm, respectively (Fig. 1). Along with the addition of a series of Zn^{2+}, the absorbance of the original three absorption bands gradually decreased. Meanwhile, the new bands at 337 nm and 428 nm became more and more prominent. And the color of the probe solution changed from colorless to light yellow (Fig. 1 inset). In addition, four isosbestic points at approximately 284 nm, 333 nm, 339 nm and 387 nm were appeared, which suggests that a new complex was formed between the probe molecule and Zn^{2+}.

The fluorescence sensitivity of probe NFC was investigated by the titration experiment of Zn^{2+}. With the increase of Zn^{2+} concentration (0–17 μM), the fluorescence intensity of the probe solution increased gradually (Fig. 2). The fluorescence signal transformation of probe NFC solution could be differentiated expediently under the UV light by the naked eye. Therefore, the probe provides a very handy tool for the easy monitoring of Zn^{2+} in water sample without expensive equipment. What's more, a good linear relationship could be established between fluorescence intensity (486 nm) and the concentration of Zn^{2+} (0–9 μM): $y = 27.97x + 39.12$ ($R^2 = 0.9912$) (Fig. 2 inset). The detection limit (DL) could also be calculated as 11.8 nM using the equation $DL = 3\sigma/S$, where σ represents the relative standard deviation of the probe solution ($\sigma = 0.11$), and S represents the slope of the linear equation ($S = 27.97$). In addition, the

complexation constant (K) between the fluorescent molecule and Zn^{2+} could also be obtained as $1.13 \times 10^5\ M^{-1}$ using the Benesi-Hildebrand equation between fluorescence intensity at 486 nm and the concentration of Zn^{2+} (Fig. 3) [36]. These results show that probe NFC can recognize Zn^{2+} with high sensitivity.

In order to investigate the detection performance of the probe, the selective experiment was also performed. The solution of probe NFC (10 μM) showed very weak fluorescence emission. After the addition of Zn^{2+} (17 μM), the fluorescence signal was significantly enhanced. Cd^{2+} ions (17 μM) only slightly increased the fluorescence intensity of the probe and in some cases may cause interference signal. However, the addition of other anlytes (17 μM), including common metal ions and anions, could not significantly change the fluorescence intensity of the probe solution except for Cd^{2+} ions (Fig. 4). Furthermore, compared with the fluorescence intensity at 486 nm of probe NFC with various analytes in the absence (black bar) and presence (red bar) Zn^{2+}, the fluorescence intensity at 486 nm of probe NFC with Zn^{2+} was not significantly disturbed by other analytes (Fig. 5). Besides, the reversible fluorescence response of probe NFC to Zn^{2+} was done using EDTA-2Na to verify the reusability. The fluorescence intensity at 486 nm of probe NFC (10 μM) was greatly enhanced after the addition of Zn^{2+} (17 μM), and it was weaken under the complexation of EDTA-2Na (20 μM). What's more, the probe remained responsive to Zn^{2+} when this reversible changes were repeated for 5 times (Fig. 6). Thus, this probe has excellent selectivity and efficient reusability for the detection of Zn^{2+}.

The response time of the probe to Zn^{2+} and the effect of pH on the detection performance of the probe were investigated, respectively. The fluorescence intensity at 486 nm of the probe solution (10 μM) was very weak, while the fluorescence intensity increased rapidly and reached immediately the maximum value after the addition of Zn^{2+} (17 μM) (Fig. 7). This indicates that the probe can realize the real-time detection of Zn^{2+}.

Additionally, the fluorescence intensity at 486 nm of probe NFC decreased markedly when pH was less than 5. This should be attributed to the fact that protons bind to probe molecules more easily than Zn^{2+}, which hinders the interaction between Zn^{2+} and probe molecules. When pH was more than 9, the fluorescence intensity of the probe also reduced significantly, due to that the presence of a large number of hydroxide ions prevented Zn^{2+} from binding to the probe molecule. As a result, the appropriate pH should be in the range of 6–8 (Fig. 8).

The effect of solution composition between CH_3CN and water on the performance of the probe was also investigated. When the volume fraction of CH_3CN was less than 20%, the fluorescence intensity difference of the probe before and after the addition of Zn^{2+} was very small. This is mostly because that excessive water leads to the aggregation of probe molecules, which not only hinders the binding of probe molecules to Zn^{2+}, but also causes fluorescence quenching. When the volume fraction of CH_3CN was greater than 30%, the fluorescence intensities (486 nm) of the probe and probe with Zn^{2+} showed a

significant difference (Fig. 9). Therefore, in the acetonitrile volume fraction greater than 30% water solutions, this probe could realize the detection of Zn^{2+}.

3.2. Complexation model and detection mechanism

To explore the detection mechanism, Job's plot was first used. The total concentration of probe NFC and Zn^{2+} was fixed at 30 μM, and the change of fluorescence intensity with the molar ratio of Zn^{2+} to probe NFC was recorded. The intersection point of the fitting curve was about 0.5, showing that probe NFC molecules bind to Zn^{2+} at a molar ratio of 1:1 (Fig. S4). This result was further confirmed by HRMS. After the addition of Zn^{2+}, the molecular peak of probe NFC at 281.0928 disappeared. And a new peak at 343.0068 appeared (Fig. S5). It was consistent with the complex peak of probe NFC and Zn^{2+} with a molar ratio of 1:1. Moreover, the hydroxyl group peak of probe NFC in ^1H NMR spectrum weakened after the interaction between the probe and Zn^{2+} (Fig. S6), indicating that hydroxyl group was involved in the coordination with Zn^{2+}. Based on the above results, the complexation model of probe NFC and Zn^{2+} was recommended (Scheme 2). For probe NFC molecule only, the photo-induced electron transfer (PET) process from C = N double bond to the naphthalene group blocked the fluorescence of the naphthalene group. When the probe molecule bonded with Zn^{2+}, the electrons of probe NFC molecule were occupied by Zn^{2+}, the PET process was destroyed, and the fluorescence of the naphthalene group was restored. In order to better illustrate the fluorescent mechanism between probe NFC and Zn^{2+}, density functional theory (DFT) was calculated using Gaussian 09 at DFT/B3LYP/6-31G (d, p) level (Fig. 10). The electron cloud of the highest occupied molecular orbital (HOMO) of the probe molecule was distributed mainly on the naphthalene group and C = N double bond, and the electron cloud of the lowest unoccupied molecular orbital (LUMO) scattered throughout the probe molecule, and their energy levels were − 5.56 eV and − 1.64 eV, respectively. However, when the probe molecule formed a complex with Zn^{2+}, the electron cloud of HOMO were concentrated around Zn^{2+} because of the strong electron-withdrawing ability of Zn^{2+}, the energy levels of HOMO and LUMO were − 3.86 eV and − 1.73 eV, respectively. Thus the PET process of probe NFC was off and the fluorescence became strong.

3.3. Application in water samples

The probe was first used for the detection of Zn^{2+} in actual water samples to evaluate its detection performance (Table 1). Zn^{2+} was not detected in the pond water and drinking water. After adding various concentrations of Zn^{2+} standard solutions, the recoveries were found to be in the range of 95.7–102.4%, and the relative standard deviation (RSD) values were in the range of 1.9–3.3%. Furthermore, this probe was used to detect Zn^{2+} contained in the commercial zinc supplement. A commercial zinc supplement solution (10 mL) contains Ca^{2+} (5.4 mg/mL), Zn^{2+} (0.43 mg/mL), lysine hydrochloride (10 mg/mL), and other excipients including NaOH, NaCl, lactic acid, saccharose and purified water. The content of Zn^{2+} contained in an oral liquid was estimated to be (0.38 ± 0.017 mg)/mL, which is close to the tagged value

of 0.43 mg/mL. These results prove that this probe can be used as an effective tool for the precise and quantitative test of Zn^{2+} in real samples.

Table 1
The detection results of Zn^{2+} using probe NFC in water samples

Sample	Spiked (μM)	Found (μM)	Recovery (%)	RSD (%)
Pond Water	0	no	no	-
	2	2.047 ± 0.044	102.4	2.2
	4	4.048 ± 0.086	101.2	2.2
	8	7.654 ± 0.153	95.7	1.9
Drinking water	0	no	no	-
	2	2.038 ± 0.065	101.9	3.3
	4	4.064 ± 0.098	101.6	2.5
	8	7.831 ± 0.186	97.9	2.3

3.4. Application in cell imaging

The detection of Zn^{2+} using this probe in living HepG2 cells was also carried out. These HepG2 cells incubated with probe NFC (10 μM) for 30 min showed very slight fluorescent emission (Fig. 4a). However, when these cells were incubated successively with probe NFC (10 μM) for 30 min, and Zn^{2+} (15 μM) for 10 min, they exhibited obvious cyan fluorescence (Fig. 4b). And this fluorescence signal and bright field cells (Fig. 4c) showed good coincidence (Fig. 4d). The cytotoxicity of probe NFC was very low by MTT test. When the concentration of the probe was no more than 30 μM, the viability of A549 cells was above 85% (Fig. S7). These results preliminarily indicate that this probe can be used for the visual detection of intracellular Zn^{2+} and has low cytotoxicity.

4. Conclusion

In summary, a fluorescent probe was conveniently synthesized using 2-hydroxy-1-naphthalene formaldehyde as the fluorophore, and furan-2-carbohydrazide as the binding group. It exhibited significant fluorescence enhancement with the participation of Zn^{2+}. And this probe has been successfully applied to the accurate and quantitative detection of Zn^{2+} in water medium, showing good selectivity, very low detection limit, real time response and reusability. The detection limit, stoichiometric ratio and binding constant (K) were also calculated to be 11.8 nM, 1:1 and $1.13 \times 10^5\ M^{-1}$, respectively. Meanwhile, the cell fluorescence imaging experiment demonstrates that this probe has the potential application to trace Zn^{2+} in living cells with low cytotoxicity.

Declarations

Availability of data and materials

The authors declare that the data supporting the findings of this study are available in the article and the supplementary materials.

Compliance with Ethical Standards

The authors declare that they have no conflict of interest. Ethical approval is not applicable. The presented research did not involve humans or animals. Informed consent is not applicable.

Competing interests

The authors have no conflicts of interest to declare that are relevant to the content of this article.

Acknowledgements

The authors would like to thank the Guangxi Science and Technology Base and Special Fund for Talents (AD19110056), Guangxi Science and Technology Department of China.

Funding

This work was supported by the Guangxi Science and Technology Base and Special Fund for Talents (AD19110056).

Author information

Affiliations

College of Chemistry and Bioengineering, Guilin University of Technology, Guilin, Guangxi, 541006, PR China.

Xinyue Mu, Liping Shi, Liqiang Yan, Ningli Tang

Corresponding authors, Liqiang Yan (E-mail: liqiangyan@glut.edu.cn) and Ningli Tang (E-mail: tangnl@glite.edu.cn).

Authors' contributions

All authors contributed to the study conception and design. Material preparation, data collection and analysis were performed by Xinyue Mu, Liping Shi, Liqiang Yan, Ningli Tang. The first draft of the manuscript was written by Liqiang Yan and all authors commented on previous versions of the manuscript. All authors read and approved the final manuscript.

Code availability

Not applicable.

References

1. J. Frederickson, J.Y. Koh, A.I. Bush, The neurobiology of zinc in health and disease, Nat. Rev. Neurosci. 6 (2005) 449–462, https://doi.org/10.1038/nrn1671.
2. Maret, Inhibitory zinc sites in enzymes, BioMetals 26 (2013) 197–204, https://doi.org/10.1007/s10534-013-9613-7.
3. K. Chesters, L. Petrie, H. Vint, Specificity and timing of the Zn2+ requirement for DNA synthesis by 3T3 cells, Exp. Cell Res. 184 (1989) 499–508, https://doi.org/10.1016/0014-4827(89)90347-9.
4. -S. Huang, Q.-B. She, K.S. Crilly, Z. Kiss, Ethanol, Zn^{2+} and insulin interact as progression factors to enhance DNA synthesis synergistically in the presence of Ca^{2+} and other cell cycle initiators in fibroblasts, Biochem. J. 346 (2000) 241–247, https://doi.org/10.1042/bj3460241.
5. Maret, Y. Li, Coordination dynamics of zinc in proteins, Chem. Rev. 109 (2009) 4682–4707, https://doi.org/10.1021/cr800556u.
6. M. Berg, Y. Shi, The galvanization of biology: a growing appreciation for the roles of zinc, Science 271 (1996) 1081–1085, https://doi.org/10.1126/science.271.5252.1081.
7. Warthon-Medina, V.H. Moran, A.-L. Stammers, S. Dillon, P. Qualter, M. Nissensohn, L. Serra-Majem, N.M. Lowe, Zinc intake, status and indices of cognitive function in adults and children: a systematic review and meta-analysis, Eur. J. Clin. Nutr. 69 (2015) 649–661, https://doi.org/10.1038/ejcn.2015.60.
8. Klaus, M. Ulrike, L.A. Tobias, H. Swen, G. Joanna, M.W. Seeliger, B. Heinrich, L. Bodo, Hyperekplexia Phenotype of Glycine Receptor α1 Subunit Mutant Mice Identifies Zn^{2+} as an Essential Endogenous Modulator of Glycinergic Neurotransmission, Neuron 52 (2006) 679–690, https://doi.org/10.1016/j.neuron.2006.09.035.
9. Tian, C.-C. He, H.-N. Xu, Y.-X. Wang, H.-G. Wang, D. An, B. Heng, W. Pang, Y.-G. Jiang, Y.-Q. Liu, Zn^{2+} reduction induces neuronal death with changes in voltage-gated potassium and sodium channel currents, J. Trace Elem. Med. Biol. 41 (2017) 66–74, https://doi.org/10.1016/j.jtemb.2017.02.011.
10. R. Williams, M. Mistry, A.M. Cheriyan, J.M. Williams, M.K. Naraine, C.L. Ellis, R. Mallick, A.C. Mistry, J.L. Gooch, B. Ko, H. Cai, R.S. Hoover, Zinc deficiency induces hypertension by promoting renal Na^{+} reabsorption, Am. J. Physiol. Renal. Physiol. 316 (2019) F646–F653, https://doi.org/10.1152/ajprenal.00487.2018.
11. S. Li, S.E. Adesina, C.L. Ellis, J.L. Gooch, R.S. Hoover, C.R. Williams, NADPH oxidase-2 mediates zinc deficiency-induced oxidative stress and kidney damage, Am. J. Physiol. Cell Physiol. 312 (2017) C47–C55, https://doi.org/10.1152/ajpcell.00208.2016.
12. J. Eide, The oxidative stress of zinc deficiency, Metallomics, 3 (2011) 1124–1129, https://doi.org/10.1039/C1MT00064K.

13. J. Tuerk, N. Fazel, Zinc deficiency, Curr. Opin. Gastroen. 25 (2009) 136–143, https://doi.org/10.1097/mog.0b013e328321b395.
14. Maywald, I. Wessels, L. Rink, Zinc Signals and Immunity, Int. J. Mol. Sci. 18 (2017) 2222, https://doi.org/10.3390/ijms18102222.
15. Xu, P. Wang, H. Wang, Z.H. Yu, H.Y. Au-Yeung, T. Hirayama, H. Sun, A. Yan, Zinc excess increases cellular demand for iron and decreases tolerance to copper in Escherichia coli, J. Biol. Chem. 294 (2019) 16978–16991, https://doi.org/10.1074/jbc.RA119.010023.
16. A. Greenberg, H.R. Briemberg, A neurological and hematological syndrome associated with zinc excess and copper deficiency, J. Neurol. 251 (2004) 111–114, https://doi.org/10.1007/s00415-004-0263-0.
17. R. Rahimzadeh, M.R. Rahimzadeh, S. Kazemi, A.A. Moghadamnia, Zinc Poisoning - Symptoms, Causes, Treatments, Mini-Rev. Med. Chem. 20 (2020) 1489–1498, https://doi.org/10.2174/1389557520666200414161944.
18. Gu, S. Yang, B. Miao, Z. Gu, J. Wang, W. Sun, D. Wu, J. Li, Electrical detection of trace zinc ions with an extended gate-AlGaN/GaN high electron mobility sensor, Analyst 144 (2019) 663–668, https://doi.org/10.1039/C8AN01770K.
19. Wolthuis, D.D. Vries, M. Poutsma, Determination of the equivalent weight of metals: A freshman research project, J. Chem. Educ. 34 (1957) 3–7, https://doi.org/10.1021/ed034p3.
20. K. Song, N.F. Adham, H. Rinderknecht, A Simple, Highly Sensitive Colorimetric Method for the Determination of Zinc in Serum, Am. J. Clin. Pathol. 65 (1976) 229–233, https://doi.org/10.1093/ajcp/65.2.229.
21. K. Dubey, B.K. Puri, Differential-pulse polarographic determination of zinc and manganese in various pharmaceutical and biological samples after adsorption of their morpholine-4-carbodithioates on microcrystalline naphthalene, Analyst 119 (1994) 1567–1570, https://doi.org/10.1039/AN9941901567.
22. K. Tewari, A.K. Singh, Thiosalicylic acid-immobilized amberlite XAD-2: metal sorption behaviour and applications in estimation of metal ions by flame atomic absorption spectrometry, Analyst 125 (2000) 2350–2355, https://doi.org/10.1039/B006788L.
23. Wang, K. Wang, Q. Kong, J. Wang, D. Xi, B. Gu, S. Lu, T. Wei, X. Chen, Recent studies focusing on the development of fluorescence probes for zinc ion, Coordin. Chem. Rev. 429 (2021) 213636, https://doi.org/10.1016/j.ccr.2020.213636.
24. Bertone, M.A. Burford, D.P. Hamilton, Fluorescence probes for real-time remote cyanobacteria monitoring: A review of challenges and opportunities, Water Res. 141 (2018) 152–162, https://doi.org/10.1016/j.watres.2018.05.001.
25. Tang, F. Pei, X. Lu, Q. Fan, W. Huang, Recent Advances on Activatable NIR-II Fluorescence Probes for Biomedical Imaging, Adv. Optical. Mater. 7 (2019) 1900917, https://doi.org/10.1002/adom.201900917.

26. Ozdemir, A selective fluorescent ‘turn-on’ sensor for recognition of Zn2+ in aqueous media, Spectrochim. Acta A. 161 (2016) 115–121, https://doi.org/10.1016/j.saa.2016.02.040.
27. Li, J. Wang, L. Xiao, J. Wang, H. Yan, A dual-response fluorescent probe for Al3+ and Zn2+ in aqueous medium based on benzothiazole and its application in living cells, Inorg. Chim. Acta. 516 (2021) 120147, https://doi.org/10.1016/j.ica.2020.120147.
28. Xiao, J. Ma, D. Li, L. Liu, H. Wang, Preparation 4'-Quinolin-2-yl-[2, 2'; 6', 2”] terpyridine as a ratiometric fluorescent probe for cadmium ions and zinc ions in aqueous, J. Photoch. Photobio. A 399 (2020) 112613, https://doi.org/10.1016/j.jphotochem.2020.112613.
29. Tang, D. Wu, Z. Huang, Y. Bian, A fluorescent sensor based on binaphthol-quinoline schiff base for relay recognition of Zn2+ and oxalate in aqueous media, J. Chem. Sci. 128 (2016) 1337–1343, https://doi.org/10.1007/s12039-016-1124-y.
30. Smita, B. Pradip Kr, D. Diganta Kumar, Condensation product of phenylalanine and salicylaldehyde: fluorescent sensor for Zn^{2+}, J Fluoresc. 26 (2016) 899–904, https://doi.org/10.1007/s10895-016-1778-3.
31. P. Algi, A simple and selective fluorescent sensor for Zn2+ and H+ ions in aqueous solution with OR logic gate function, J. Fluoresc. 26 (2016) 1083–1089, https://doi.org/10.1007/s10895-016-1798-z.
32. Lin, T. Chen, C. Liu, A. Wu, A Fluorescent chemosensor based on naphthol for detection of Zn2+, Luminescence 31 (2016) 236–240, https://doi.org/10.1002/bio.2951.
33. Liu, Y. Tan, Q. Hu, Y. Wang, X. Wu, Q. Huang, W. Zhang, M. Zheng, H. Wang, A naked eye fuorescent chemosensor for Zn2+ based on triphenylamine derivative and its bioimaging in live cells, Chem. Pap. 73 (2019) 3123–3134, https://doi.org/10.1007/s11696-019-00853-3.
34. Han, X. Zhang, Z. Li, Y. Gong, X. Wu, Z. Jin, C. He, L. Jian, J. Zhang, G. Shen, R. Yu, Efficient fluorescence resonance energy transfer-based ratiometric fluorescent cellular imaging probe for Zn2+ using a rhodamine spirolactam as a trigger, Anal. Chem. 82 (2010) 3108–3113, https://doi.org/10.1021/ac100376a.
35. K. Walkup, S.C. Burdette, S.J. Lippard, R.Y. Tsien, A new cell-permeable fluorescent probe for Zn2+, J. Am. Chem. Soc. 122 (2000) 5644–5645, https://doi.org/10.1021/ja000868p.
36. Yan, S. Zhang, Y. Xie, C. Lei, A fluorescent probe for Gallium (Ⅲ) ions based on 2-hydroxy-1-naphthaldehyde and L-serine, Dyes Pigm. 175 (2020) 108190, https://doi.org/10.1016/j.dyepig.2020.108190.

Figures

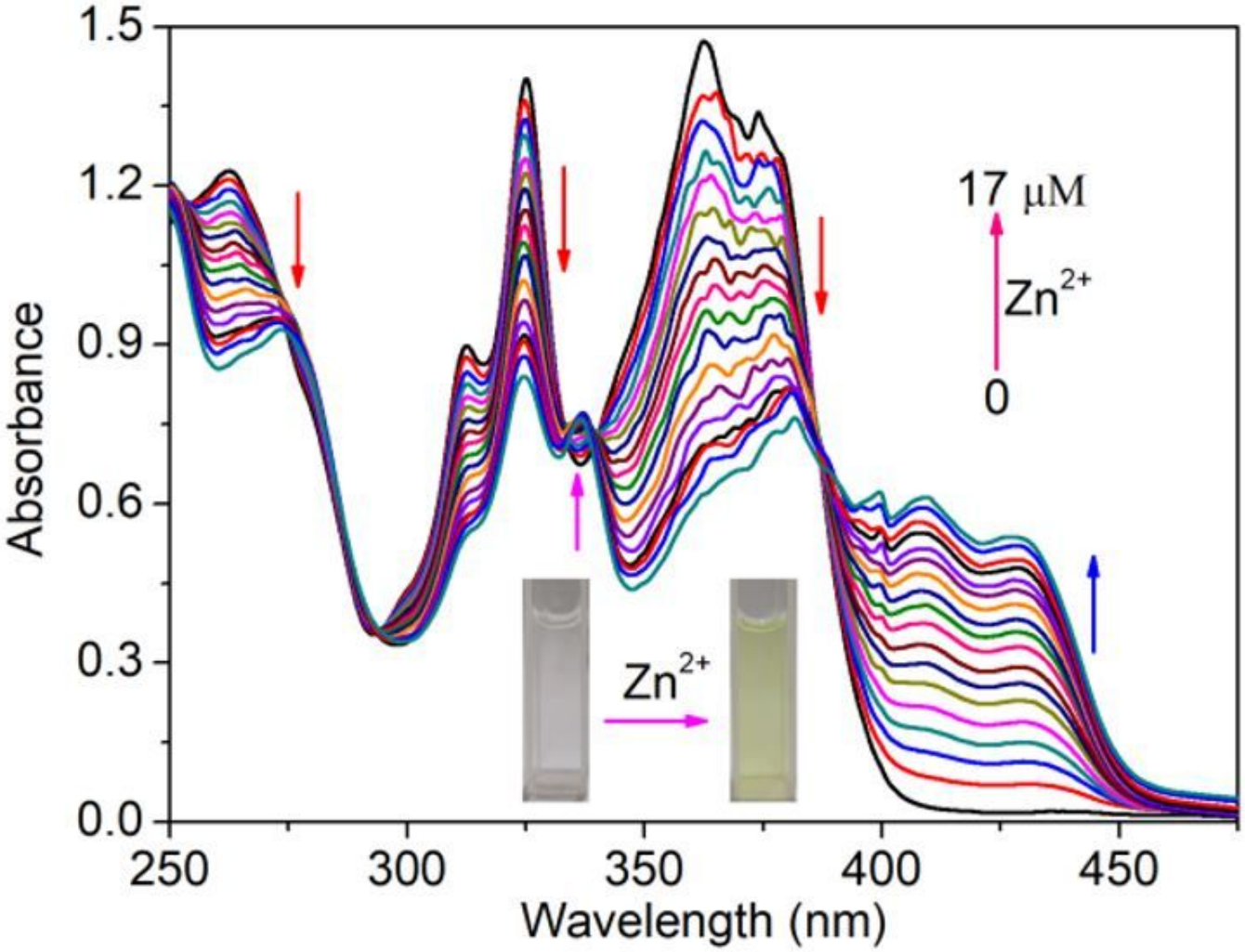

Figure 1

UV-Vis spectra of probe NFC (10 μM) with different content of Zn2+. Inset: images of probe NFC (10 μM) without and with Zn2+ (17 μM).

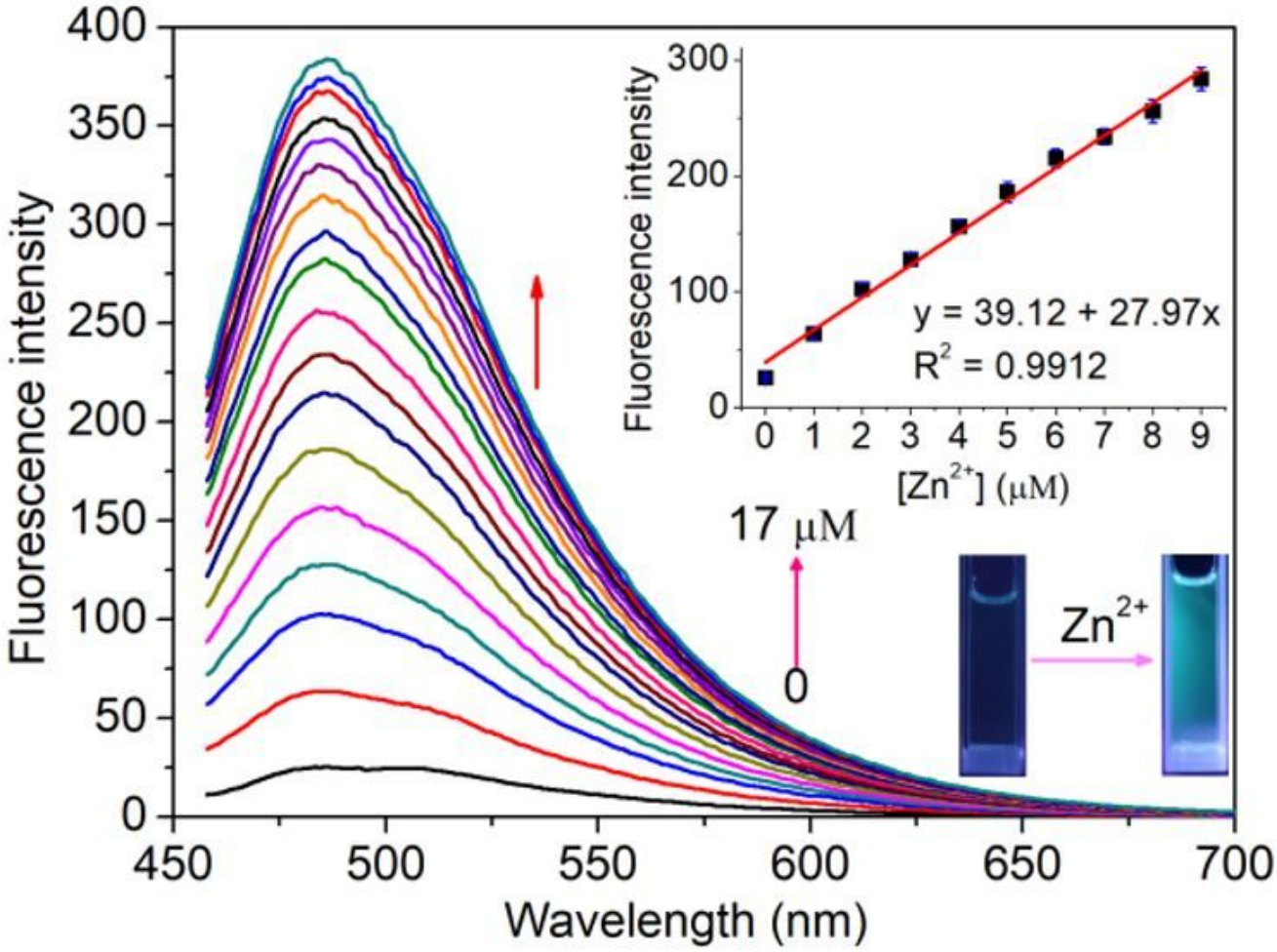

Figure 2

Fluorescence spectra of probe NFC with a series of Zn2+. Inset: The linear relationship between fluorescence intensity at 486 nm and the concentration of Zn2+ ions (0 – 9 μM), and images of probe NFC (10 μM) without and with Zn2+ (17 μM).

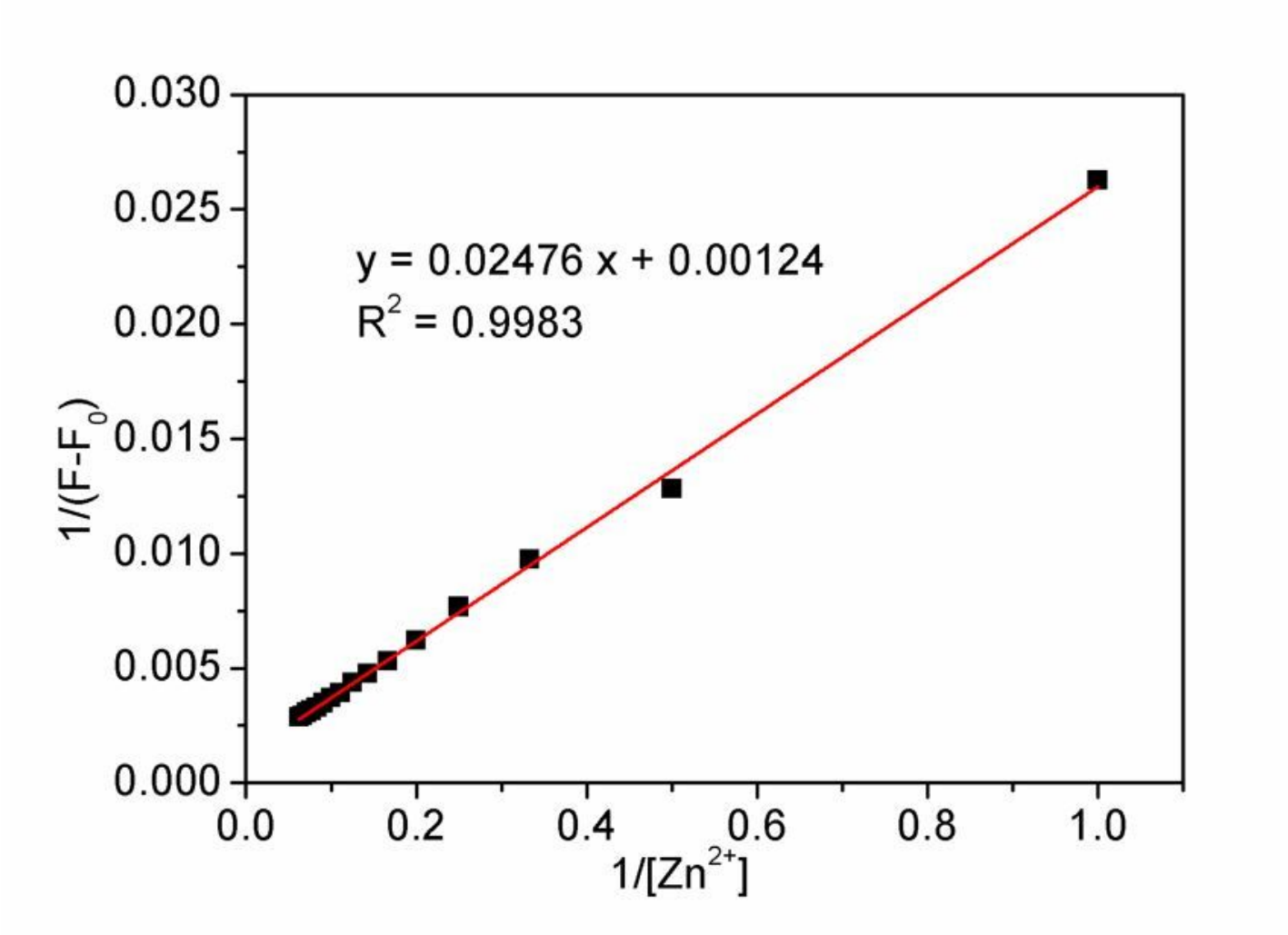

Figure 3

Benesi-Hildebrand equation between fluorescence intensity at 486 nm and the concentration of Zn2+.

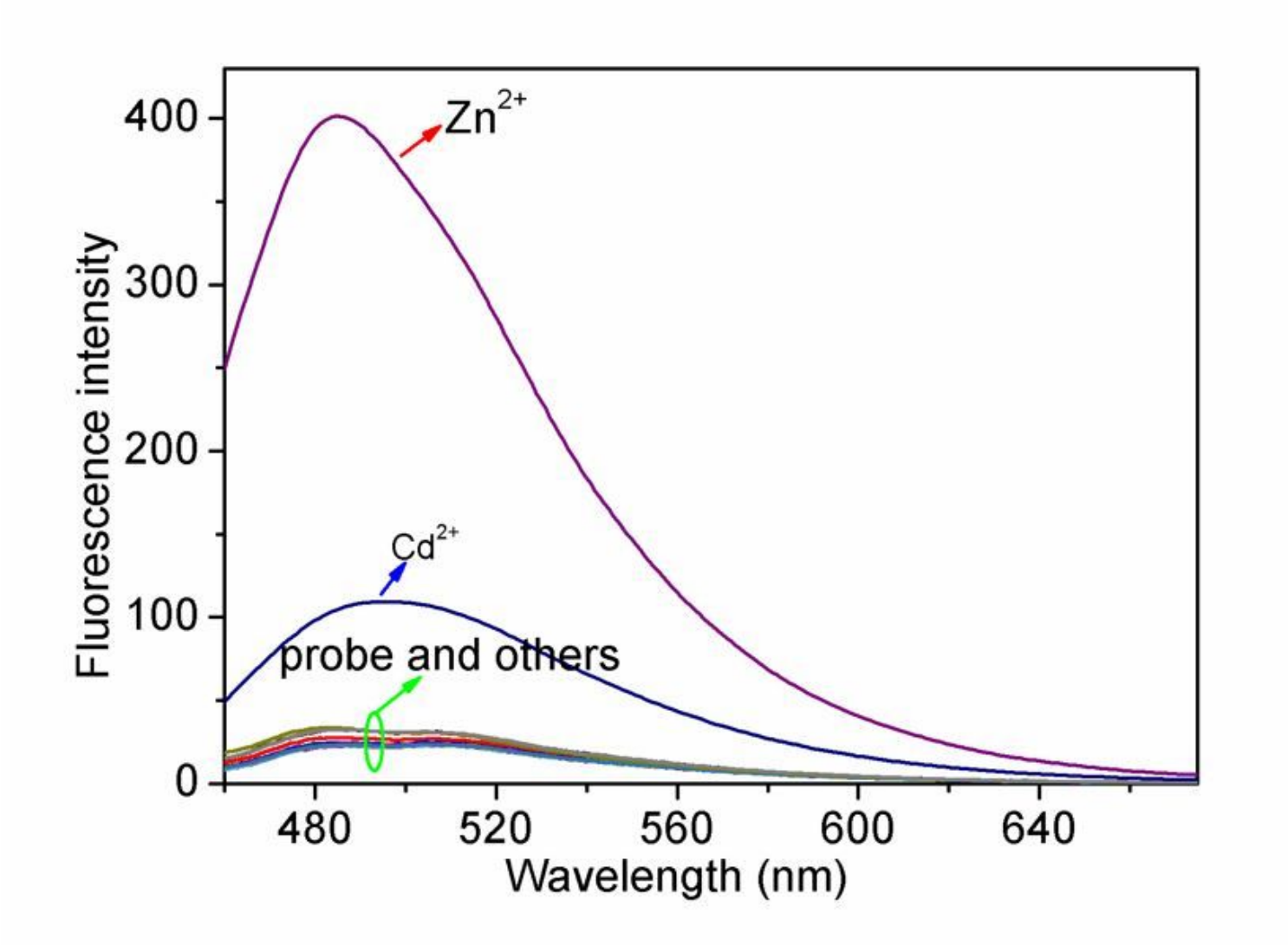

Figure 4

Fluorescence spectra of probe NFC with various analytes.

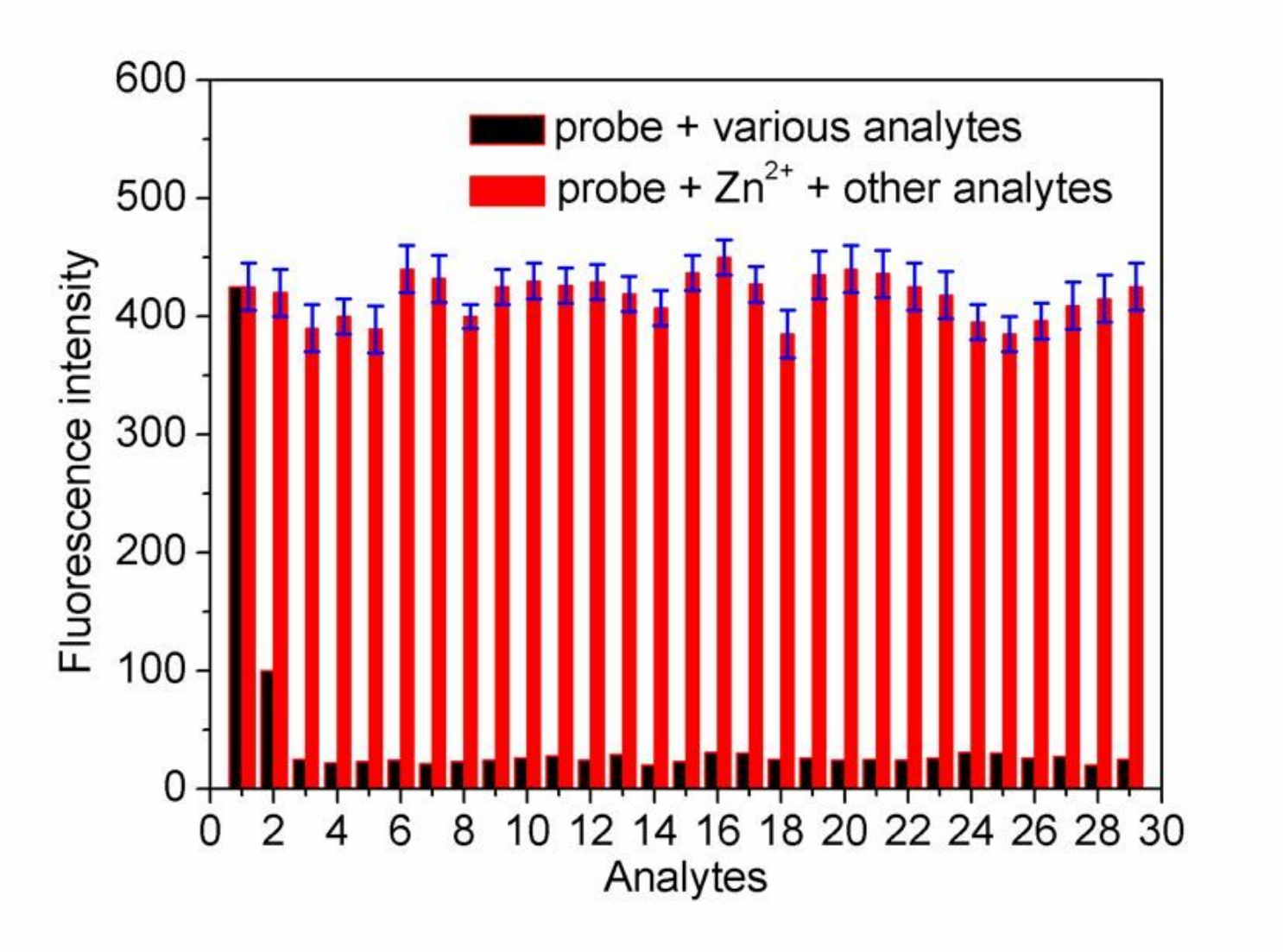

Figure 5

Fluorescence intensity at 486 nm of probe NFC with various analytes in the absence and presence of Zn2+. (1) Zn2+, (2) Cd2+, (3) Ni2+, (4) Co2+, (5) Cu2+, (6) Ca2+, (7) Mg2+, (8) Pb2+, (9) Hg2+, (10) Ba2+, (11) Fe2+, (12) Li+, (13) Na+, (14) K+, (15) Ag+, (16) Al3+, (17) Cr3+, (18) Fe3+, (19) F-, (20) Cl-, (21) Br-, (22) SO32-, (23) SO42-, (24) NO3-, (25) NO2-, (26) PO43-, (27) CO32-, (28) S2O32-, (29) Ac-.

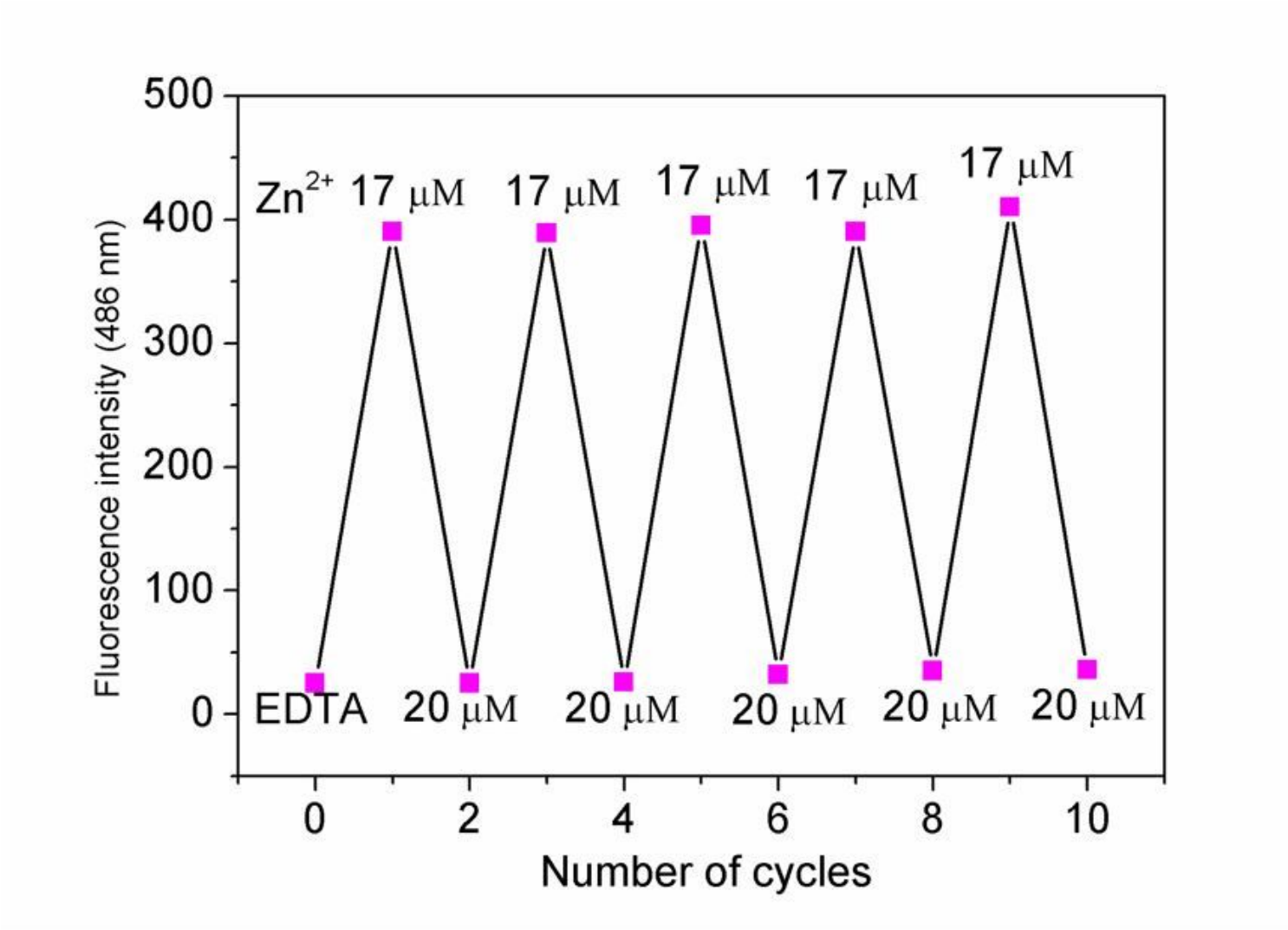

Figure 6

Reversible changes in the fluorescence intensity (486 nm) of probe upon the sequential addition of Zn2+ and EDTA.

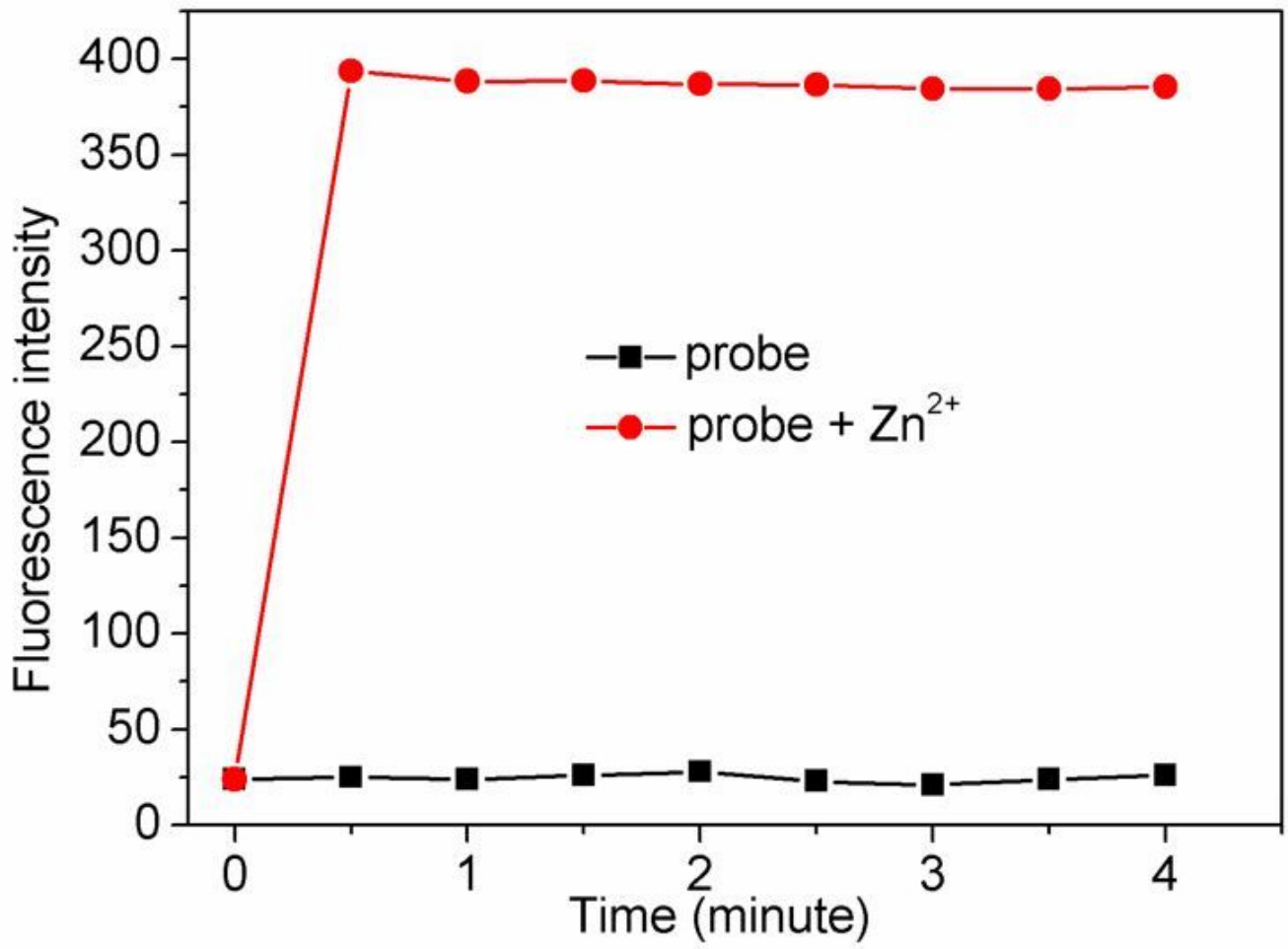

Figure 7

Change trend of fluorescence intensity (486 nm) of the probe with time before and after adding Zn2+ ions.

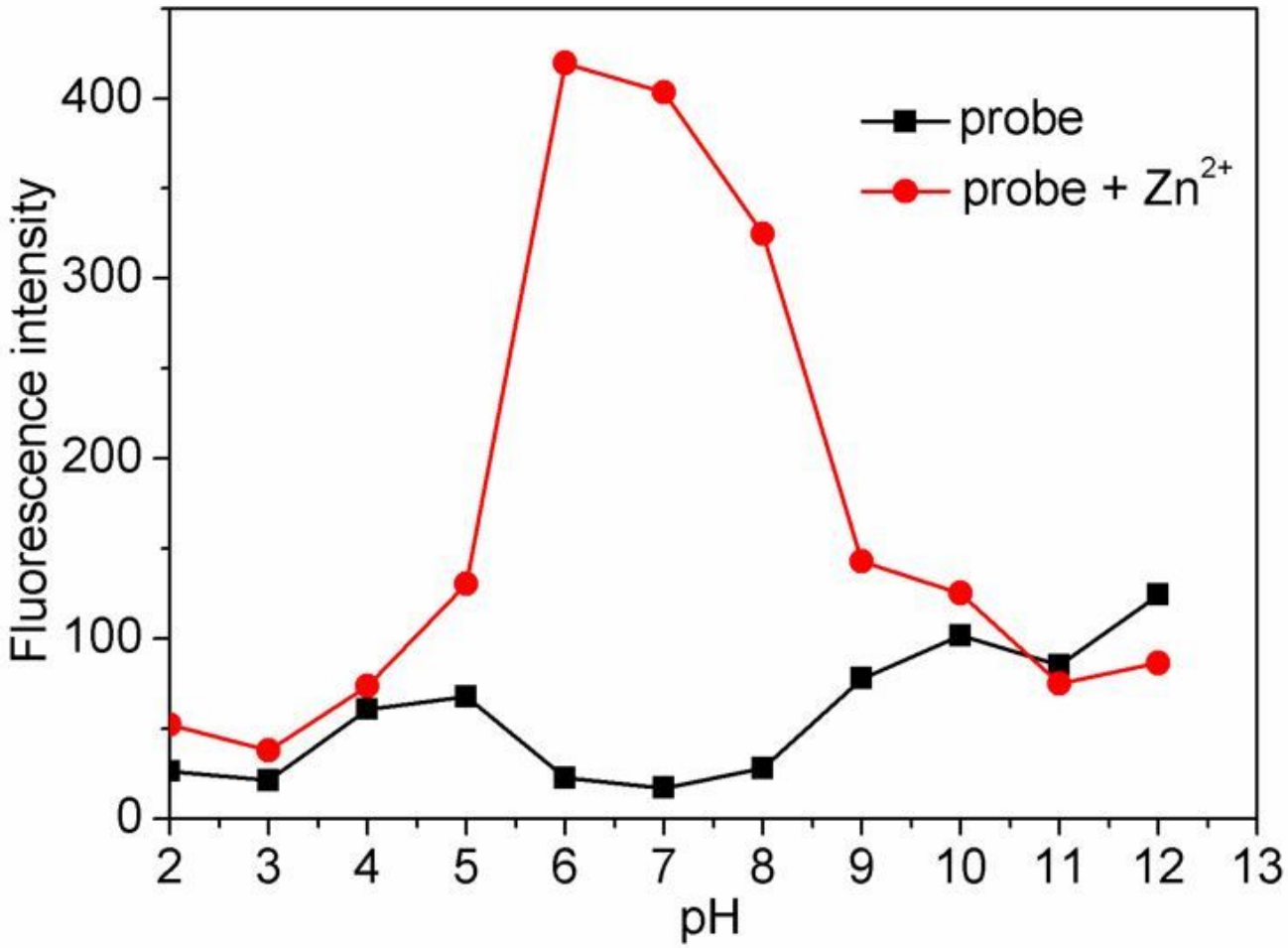

Figure 8

Change trend of fluorescence intensity (486 nm) of the probe with pH values before and after adding Zn2+ ions.

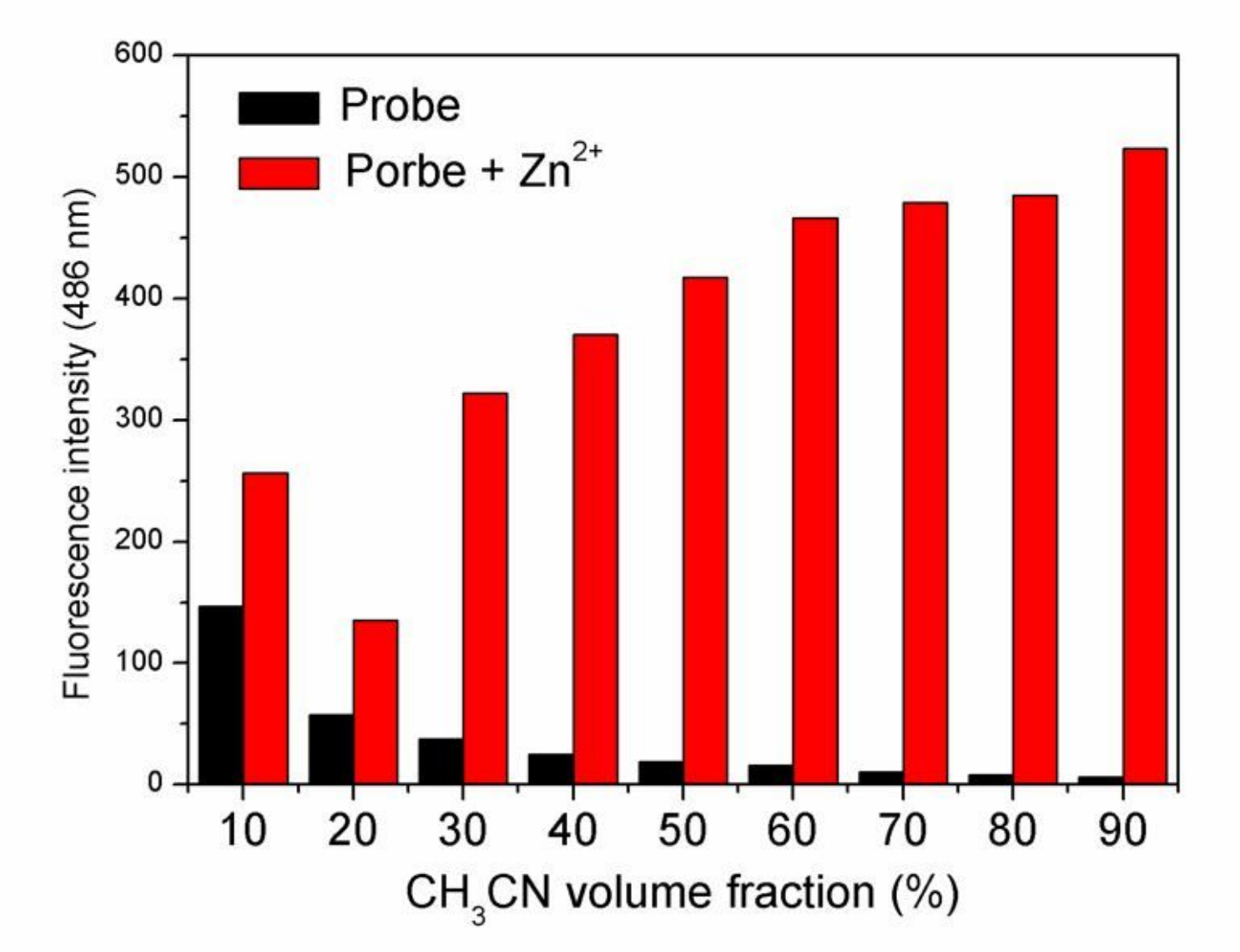

Figure 9

Change trend of fluorescence intensity (486 nm) of the probe with volume fraction of CH3CN before and after adding Zn2+ ions.

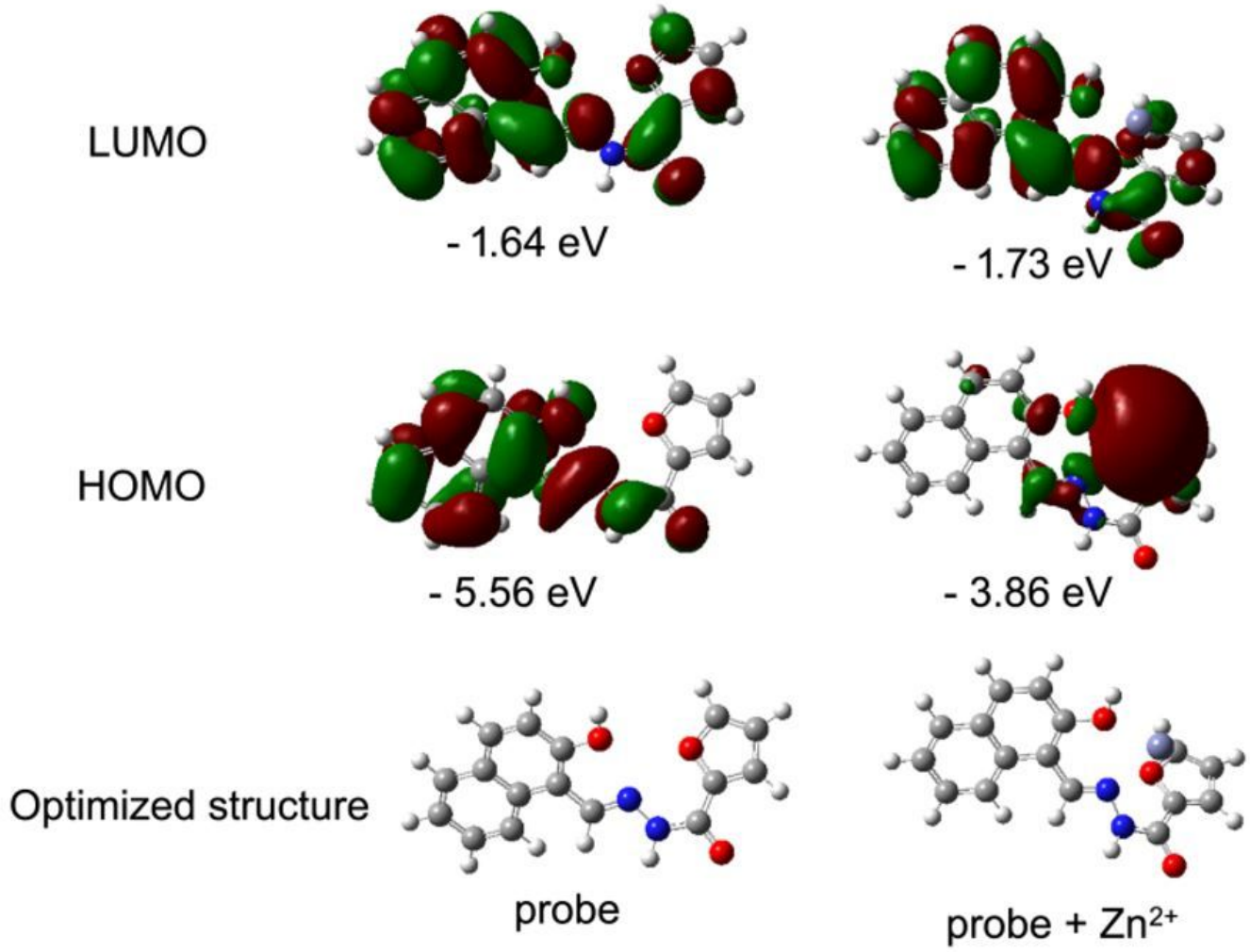

Figure 10

Optimized structures and molecular orbitals of probe and probe + Zn2+ calculated by using B3LYP/6-31 G (d, p) as implemented on Gaussian 09.

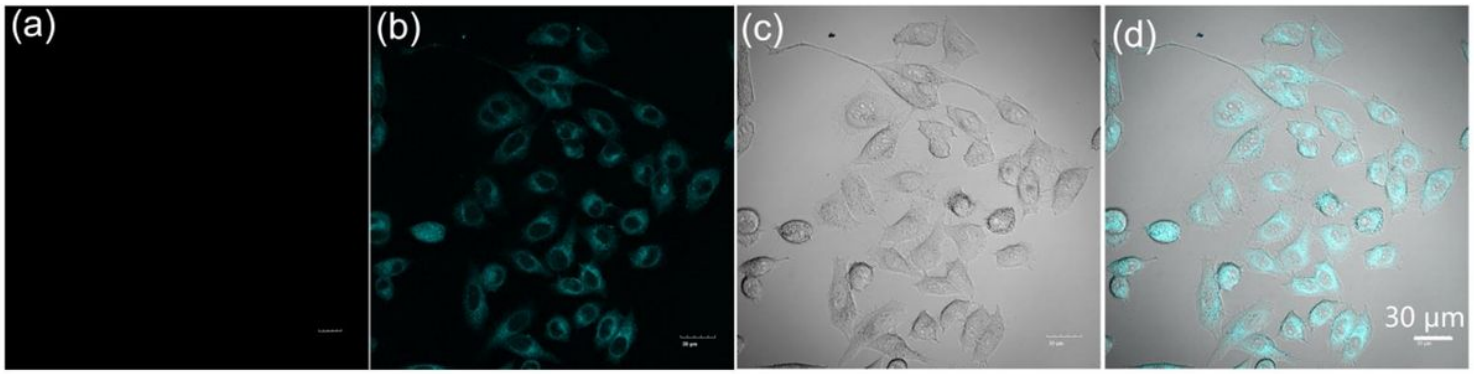

Figure 11

(a) Fluorescence image of HepG2 cells incubated with probe NFC (10.0 μM); (b) Fluorescence image and (c) bright field image of HepG2 cells incubated successively with probe NFC (10 μM) and Zn2+ (15 μM); (d) Overlay image of image b and c.

Supplementary Files

This is a list of supplementary files associated with this preprint. Click to download.

- scheme1.jpg
- scheme2.jpg